The Journal of Experimental Biology 204, 2073–2085 (2001)
Printed in Great Britain © The Company of Biologists Limited 2001
JEB3170

SHAPE, FLAPPING AND FLEXION: WING AND FIN DESIGN FOR FORWARD FLIGHT

S. A. COMBES* AND T. L. DANIEL
Department of Zoology, University of Washington, Seattle, WA 98195, USA
*e-mail: scombes@u.washington.edu

Accepted 22 March 2001

Summary

Both kinematics and morphology are critical determinants of performance in flapping flight. However, the functional consequences of changes in these traits are not yet well understood. Traditional aerodynamic studies of planform wing shape have suggested that high-aspect-ratio wings generate more force per area and perform more efficiently than low-aspect-ratio wings, but these analyses may neglect critical components of flapping flight such as unsteady fluid dynamics and wing or fin flexion. In this paper, we use an unsteady potential flow analysis that incorporates wing flexion to test predictions of optimal wing shape under varying degrees of unsteady motion and wing flexion. We focus on forward flapping flight and examine the effects of wing/fin morphology and movements on thrust generation and efficiency. We test the model by comparing our predictions with kinematic data derived from the aquatic flight of the ratfish *Hydrolagus colliei*. Our analyses show that aspect ratio and the proportion of area in the outer one-fifth of the wing can characterize wing shape in terms of aero- or hydrodynamic performance. By comparing the performance of wings that vary in these two parameters, we find that traditional predictions of optimal wing shape are valid only under limited circumstances (when flapping frequency is low, wings are stiff or wings are tapered at the tips). This indicates a complex relationship between locomotor traits and performance and helps explain the diversity of wing kinematics and morphologies observed in nature.

Key words: locomotion, wing shape, flexion, unsteady effect, flapping flight, aquatic flight, swimming, ratfish, *Hydrolagus colliei*.

Introduction

Swimming and flying animals generate fluid-dynamic forces by flapping flexible appendages such as wings or fins. The stresses generated by motions of these structures can be resolved into vertical forces that support an animal's weight and horizontal forces that provide thrust for forward motion. Both aerial and aquatic animals that propel themselves with wing-like appendages generate these vertical and horizontal forces. Aerial animals, which must support their weight, generate a larger net upward force than aquatic animals, which often generate vertical forces that cancel over a stroke. Despite such differences, the principles governing fluid flow around a flapping appendage remain the same. The key issues involve understanding how the motion and shape of an appendage determine the timing and magnitude of forces derived from the various fluid stresses.

These structural and kinematic traits determine the locomotor performance of flying and swimming animals. Locomotor performance can have an enormous impact on an animal's survival by providing varying levels of speed, maneuverability and endurance in escaping from predators, capturing prey or foraging for food. The large variety of wing morphologies and kinematics observed in flying animals (both aerial and aquatic forms) suggests that no single 'optimal' combination of locomotor traits exists, but rather that different performance requirements lead to different combinations of these traits.

Attempts to explain the diversity of locomotor traits in flying and swimming animals require an understanding of the functional consequences of changes in morphology and kinematics. Two features of wing morphology that are likely to affect performance are planform wing shape and wing flexion. Both may be altered by active muscular bending and passive deformation of wings arising from inertial and fluid-dynamic loads. These traits, along with the time-dependent flow phenomena that result from the kinematics of flapping, contribute to crucial details of the flow and, thus, to the magnitude of instantaneous fluid-dynamic stresses on the wing.

Wing planform shape, in particular, has commonly been associated with locomotor performance during steady flight because of the higher induced drag associated with low-aspect-ratio wings (aspect ratio=span^2/area). Low-aspect-ratio wings generally have blunter tips and, thus, may lose more circulation in this region (manifest as tip vortices). This results in a backward tilt to the force vector, or induced drag. Thus, predictions derived from steady-state aerodynamics suggest that long, thin wings (with a high aspect ratio and less induced

drag) can produce more force per area and perform more efficiently than low-aspect-ratio wings (for a review, see Spedding, 1992).

These results are, at first glance, disconcerting in that they seem to suggest that selection for locomotor performance would drive wings, as well as fins that generate force by lift-based mechanisms, to become more similar through time and eliminate the morphological variation seen in nature. This view is often countered with suggestions that low-aspect-ratio wings have, generally, a lower wing loading and thus that the mechanical stresses may be lower. Similarly, there is a notion that exceedingly high-aspect-ratio wings are prohibited by the mechanical limits of the wing and fin structures that support the animal's weight.

In addition, these steady-state predictions of optimal wing shape may change when unsteady motions such as flapping are considered. As flapping frequency increases, the magnitude of bound circulation on the wing and the forces that result from this circulation decrease (because circulation has less time to develop before stroke reversal). Alternatively, accelerational forces rise with increasing unsteadiness. Finally, while not a focus here, novel unsteady mechanisms such as clap-and-fling, leading-edge vortices, wake capture and rotational circulation (e.g. Dickinson et al., 1999; Ellington, 1995; Ellington et al., 1996) will further complicate simple analyses of wing shape.

Moreover, it is important to realize that aspect ratio provides a rather crude description of wing shape in that it reflects only the average chord length (l_{avg}) in wings of the same area. Wings with the same average chord length and total area can have that area distributed quite differently, and their aerodynamic performance can vary widely in response to that shape distribution (Ellington, 1984b).

The functional consequences of wing shape, wing flexion and unsteady motion could most easily be understood by examining changes in the pressure distribution over flapping wings during flight. In the absence of appropriate technology, however, one must resort to a variety of alternative experimental approaches. Physical measurements of the forces generated during animal flight generally either average the forces over a wingbeat (e.g. wake analysis, Ellington, 1984c; Rayner, 1979) or sum steady forces for each time step of a flap (e.g. quasi-steady analysis, Blake, 1983a; Blake, 1983b; Blake, 1983c; Clark and Bemis, 1979; Ellington, 1984a; Pennycuick, 1972; Webb, 1973; Weis-Fogh, 1975). Other techniques such as flow visualization and simulation *via* physical or robotic models have been used to test theoretical analyses of flight and to suggest novel mechanisms underlying the fluid dynamics of swimming and flight (Dickinson, 1996; Dickinson et al., 1999; Ellington et al., 1996), but have not yet been used in a broad, comparative context.

Efforts are increasingly focusing on computational methods for solving the Navier–Stokes equations and calculating force production (e.g. Liu et al., 1998, and the immersed elastic boundary method of Peskin, 1995). While these approaches can validate theories of flight and suggest novel mechanisms, they are computationally intensive and thus may restrict the range of variables one can explore. For this reason, a simpler analytical model that accounts for important morphological and kinematic features is a valuable tool that can be used to identify critical features that warrant further examination.

In this paper, we investigate factors that may influence the evolution of flapping wings and fins using an unsteady potential flow analysis and measured kinematics to calculate the forces produced by a flapping wing. This analysis predicts the forces generated by pressure differences across the surface of a wing resulting from acceleration- and circulation-based phenomena. It accounts for unsteady effects such as added-mass forces and the growth of bound circulation. Because the analysis requires that fluid leave the wing smoothly at the trailing edge (the Kutta condition), it does not predict forces derived from separated flow, attached vortices or fast rotations at stroke reversal. While the model assumes that fluid is inviscid (and therefore does not apply to animals moving at low Reynolds numbers), it is appropriate for a broad range of aerial and aquatic animals in forward, flapping flight.

A critical feature of the analysis is its inclusion of chordwise wing flexion, specified by a rearward traveling wave on the wing. In a flexing wing or fin, the peak of this wave corresponds to the highest point (maximum amplitude) in the stroke, and wave speed represents the speed at which this peak travels from the leading to the trailing edge as the wing bends at stroke reversals. In a flexible wing with no active control, wave speed will be low (because the wing bends considerably at stroke reversals), while in a stiff wing, wave speed will be high because the entire wing reaches the point of stroke reversal at nearly the same time.

Defining flexion by a traveling wave, rather than by flexural stiffness or a spring constant, allows the model to be applied not only to animals whose wings or fins bend passively as a result of inertial forces, but also to those that actively pass waves rearward on their appendages (e.g. skates; see Daniel, 1987). A similar approach has been used by Tong et al. (Tong et al., 1993) to analyze the performance of a variety of caudal fin shapes; these are quite unlike the shapes of the wings and lift-generating pectoral fins that constitute the focus of this study.

We examine underwater flight in the spotted ratfish (*Hydrolagus colliei*) to test the model. This animal relies entirely on flapping its large, flexible pectoral fins for routine locomotion. We chose the ratfish because it affords a number of advantages. The relatively modest amplitude of fin motions and low reduced frequency at which they operate suggest that the Kutta condition is satisfied. In addition, the presence of a measurable chordwise bending pattern on the fin permits us to examine the consequences of wing deformation.

Fin flexion in the ratfish may be the result of passive and/or active processes. The muscles controlling the pectoral fin do not extend out into the fin rays, but the muscles at the fin base may fire in temporal succession (Bestor, 1993), conferring some degree of active control. Because the model we use describes wing flexion by a physically observed wave speed,

it is not necessary to unravel the contributions of active and passive flexion to calculate hydrodynamic forces.

We ask three questions. (i) Can an unsteady potential flow model that incorporates wing flexion reasonably predict performance (measured in terms of power, thrust and efficiency) in forward, flapping flight? (ii) What variables can be used to classify wing shape in terms of locomotor performance? (iii) What is the relative performance of wings with different shapes under varying levels of unsteady motion and wing flexion?

Although traditional aerodynamic analyses find that high-aspect-ratio wings perform better, previous work with the unsteady potential flow analysis has suggested that unsteady effects and wing flexion may be important additional factors that affect the performance of various wing shapes (Daniel, 1987). A better understanding of how these factors interact may provide insight into the functional consequences of the diverse wing morphologies and kinematics seen in nature.

Materials and methods

Calculation of fluid forces

The motion of a flexible, flapping wing can be approximated by a three-dimensional harmonically oscillating surface (Daniel, 1987; Wu, 1971). The motion of this surface is given by the following equation for a wing centered on the origin (for a movie of the motion simulated by Equation 1, see http://faculty.washington.edu/danielt/Wingmovies.html):

$$h(x,z,t) = \xi z\,\{[h_0 + \varepsilon(x+1)]\exp\{i\omega[t-(x+1)/c]\} - [\gamma(x+1)]\}, \quad (1)$$

where the function $h(x,z,t)$ describes the instantaneous location of all points on the wing. The wing coordinates in the spanwise (x) and chordwise (z) directions are both dimensionless ($-1 \leqslant x \leqslant 1$; $0 \leqslant z \leqslant 1$); t is time. The amplitude of the leading-edge oscillation at any given point along the span is described by h_0, and linear amplitude variation in the spanwise direction is specified by ξ. The circular frequency of wing oscillation is described by ω ($\omega=2\pi f$, where f is the flapping frequency); i is $\sqrt{-1}$. A traveling wave of deformation moves rearward at speed c, simulating the bending that results from flapping a flexible structure such as a wing or fin. Linear amplitude variation in the chordwise direction is given by ε, and the mean angle of attack averaged over a stroke is specified by γ.

To compute the fluid forces generated by a flapping wing, we divide the wing into chordwise strips and treat each strip as a harmonically oscillating flexible plate with its motion prescribed by Equation 1. We calculate the fluid forces generated by this segment with a two-dimensional solution to Euler's equation (Daniel, 1987; Wu, 1971), and sum the strips to determine the total fluid forces (Daniel, 1987).

The harmonic motion of flapping wings underlies an important non-dimensional measure of unsteady motion, the reduced frequency parameter ($\sigma=\omega l/U$, where l is a characteristic length, e.g. half chord length, and U is the forward velocity); this parameter describes the amount of vertical oscillation relative to forward steady motion. Because the growth of circulation around the wing is time-dependent (Dickinson, 1996; Dickinson et al., 1999; Ellington, 1995; Fung, 1990), increases in the reduced frequency parameter lead to a reduction in bound circulation and a temporal lag between wing motion and force generation. At the same time, however, this increased unsteadiness generates larger accelerations and inertial forces. Thus, pressures across the wing are not related to the reduced frequency parameter in any simple way.

All these effects are absorbed into four coefficients: the coefficient of power (C_P), which describes the rate at which energy is expended to produce thrust and create vorticity in the wake, the coefficient of energy (C_E), which describes the rate of energy loss to the wake, the coefficient of thrust (C_T), which is defined as the difference between the rates of energy expenditure and energy loss ($C_P - C_E$), and an efficiency parameter (η), defined as the ratio of useful work done (thrust produced) to power expended (C_T/C_P) (Daniel, 1987; Wu, 1971; see Appendix 1).

From these dimensionless coefficients, the power expended by a chordwise strip of the wing can be calculated:

$$P_{\text{strip,i}} = \tfrac{1}{4}\rho C_{\text{P,i}} U^3 S_{\text{i}}, \quad (2)$$

where ρ is fluid density, S_{i} is the area of strip i ($S_{\text{i}}=2l_{\text{i}}w_{\text{i}}$, where l_{i} is the half-strip length and w_{i} is the strip width). Similarly, thrust can be calculated for each strip as:

$$T_{\text{strip,i}} = \tfrac{1}{4}\rho C_{\text{T,i}} U^2 S_{\text{i}}. \quad (3)$$

These measures for each strip of the wing, with its unique motions, chord length and area, can be summed and multiplied by 2 (to account for both wings) to give the total power and thrust generated:

$$P_{\text{total}} = 2\sum_{i=1}^{n} (\tfrac{1}{4}\rho C_{\text{P,i}} U^3 S_{\text{i}}), \quad (4)$$

$$T_{\text{total}} = 2\sum_{i=1}^{n} (\tfrac{1}{4}\rho C_{\text{T,i}} U^2 S_{\text{i}}), \quad (5)$$

where n is the number of strips in each wing.

The Froude efficiency of a strip (η) is defined as:

$$\eta_{\text{strip,i}} = (T_{\text{strip,i}}U)/P_{\text{strip,i}} = C_{\text{T,i}}/C_{\text{P,i}} \quad (6)$$

and the total efficiency of the wings is:

$$\eta_{\text{total}} = (T_{\text{total}}U)/P_{\text{total}} = \sum_{i=1}^{n} (\tfrac{1}{4}\rho C_{\text{T,i}} U^2 S_{\text{i}})U \Big/ \sum_{i=1}^{n} (\tfrac{1}{4}\rho C_{\text{P,i}} U^3 S_{\text{i}}). \quad (7)$$

Ratfish kinematics and modeling

We collected spotted ratfish (*Hydrolagus colliei*; Lay and Bennett, 1839) by trawling near the San Juan Islands in Puget Sound, Washington, USA, and maintained the fish in a large,

covered outdoor tank with a continuous flow of fresh sea water. We filmed the animals swimming at constant velocity in a continuous-flow flume with a working area of 97 cm×34 cm×36 cm. Two Hi-8 video cameras filming at 30 frames s^{-1} recorded simultaneously the lateral view and the dorsal view, which was reflected by a mirror placed at 45° to the top of the flume. We filmed at flow speeds of 0.08–0.15 m s^{-1}, speeds that induced the ratfish to swim but allowed them to maintain position in the flume.

We analyzed the kinematics of two ratfish, a large female and a juvenile, to represent the extremes in size of this species. From the lateral view, we measured fin tip amplitude, flapping frequency and wave speed (Fig. 1). We computed tip amplitude (H) by averaging over 21 half-strokes in a continuous sequence for the female and over six half-strokes in two sequences for the juvenile. We measured the period (τ) of a flap and calculated flapping frequency (f=1/τ) in the adult female over 17 complete flaps in two sequences and in the juvenile over 2.5 flaps in one sequence.

We determined wave speed (c) by recording the total time required for a wave peak (bend) to travel from the leading edge (near the fin base) to the trailing edge and dividing this time by the length of the base. We measured wave speed only at the end of the upstroke, as this is when the wave is most visible, and calculated an average wave speed for each fish (over 17 upstrokes in two sequences for the female and four upstrokes in two sequences for the juvenile).

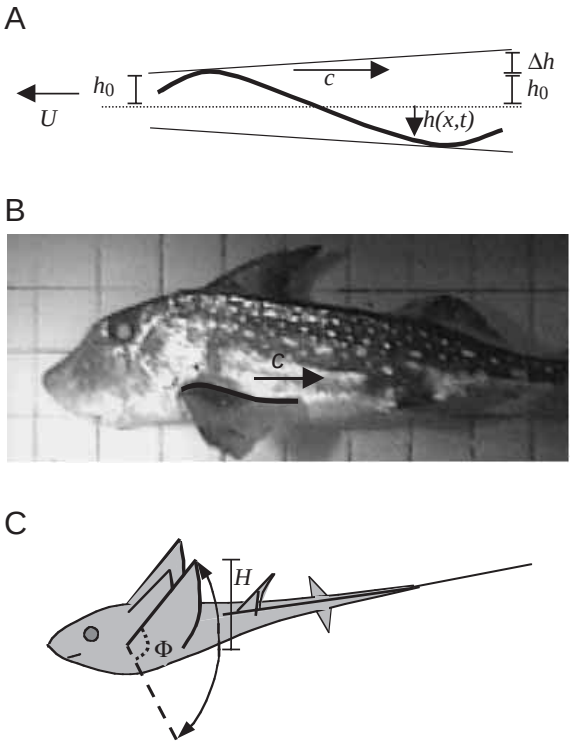

Fig. 1. (A) Two-dimensional strip oscillating with amplitude h_0 and moving forward at velocity U while a wave passes rearward at velocity c. The amplitude changes from the leading to the trailing edge by a factor ε, the ratio of Δh to h_0. The instantaneous location of a point (x) on the strip is described by $h(x,t)$, where t is time. (B) A ratfish with a wave (highlighted) traveling backwards on its pectoral fin at wave speed c. (C) Diagram of a ratfish illustrating the angle (Φ) subtended by a flapping fin and tip amplitude (H).

We analyzed chordwise amplitude change (ε) in the two fish by comparing the amplitude of the leading and trailing edges at several different spanwise positions (measured in four frames in the female and six frames in the juvenile). In addition, we measured the amplitude of several points on the leading edge and plotted amplitude against spanwise position to determine whether there was any significant spanwise bending.

We measured span (z_0), the total area of one pectoral fin (S_p) and chord length distribution along the span (Fig. 2A) in dorsal views of the female and juvenile. From these measurements, we calculated the aspect ratio of each fish's pectoral fins. We also used span and tip amplitude to calculate the angle (Φ) subtended by the flapping fin (Fig. 1C).

We calibrated the measurements made from video images with a grid on the back wall of the flume, and scaled our results in each frame by the distance of the fish from this wall (as revealed by the dorsal view). To avoid edge effects, we did not analyze sequences in which the ratfish was touching the sides or bottom of the flume.

We used the measured parameters in the potential flow model described above (with 10 chordwise strips) and compared the calculated thrust with an estimate of drag on a ratfish body and fins because drag should equal thrust when an animal is swimming at constant velocity. We obtained drag coefficients for a ratfish body ($C_{D,body}$=2.54) and fin ($C_{D,fin}$=0.28) from Sullivan (Sullivan, 1979), who measured forces on submerged ratfish bodies (with fins removed) towed at a fixed velocity and drag on an isolated fin with force transducers in a steady-flow flume.

We used these coefficients to calculate the total drag on the body and both fins of swimming ratfish as:

$$D_{body} = (\tfrac{1}{2}\rho C_{D,body} U^2 S_{cs}), \quad (8)$$

$$D_{fins} = 2(\tfrac{1}{2}\rho C_{D,fin} U^2 S_p), \quad (9)$$

where S_{cs} is the maximum cross-sectional area of the fish's body.

We also calculated the forces produced by a flapping ratfish fin with a wave speed of 100 m s^{-1} to simulate a stiff pectoral fin. Comparing these results with the forces produced by a fin with the measured wave speed demonstrates the effects of fin flexion on calculated force production.

Generation of theoretical wing shapes

To compare the performance of wings with different planform shapes, we generated a variety of theoretical wings with mathematical equations (see Appendix 2). We divided the wings into 30 chordwise strips and calculated fluid forces generated by the wings when flapping with identical kinematics. By conserving wing area throughout our simulations, we were able to examine changes in performance due purely to the redistribution of area.

We fixed span (as well as area) to create sets of theoretical wings that have the same aspect ratio, but vary in their chord length distribution and in their apparent shape (Fig. 2B–F). By using several different equations to generate the wings, we were able to examine the effects of subtle differences in wing shape on flight performance.

Wing shape parameters and relative performance of theoretical wings

Before comparing the performance of theoretical wings, we asked whether wings could be classified by general shape parameters. We focused on two shape parameters: aspect ratio and the proportion of area in the outer part of the wing. Aspect ratio provides a useful description of how long and skinny wings are on average (in wings of the same area, aspect ratio essentially describes the average chord length of the wing, l_{avg}; average chord length increases as aspect ratio decreases), but aspect ratio does not contain any information about how area is distributed within the wing. The proportion of area in the outer part of the wing is a simple measure of how area is distributed, but may provide valuable information; in flapping wings where the stroke amplitude increases spanwise, the outer part of the wing undergoes greater accelerations and, thus, may contribute more to unsteady force production.

To determine whether the proportion of area in the outer part of the wing is a useful shape parameter, we examined the relationship between performance (thrust and efficiency) and the amount of area in the outer part of the wing in a variety of wings with fixed area and aspect ratio. We also compared the performance of wings that have similar values of both shape parameters, but slightly different chord length distributions (because they were generated by different equations). If the two shape parameters are sufficient to describe wing shape in terms of aerodynamic performance, these wings should perform similarly. We examined the effects of aspect ratio on performance by changing aspect ratio while the proportion of area in the outer part of the wing remained fixed, and varied flapping frequency and wave speed to determine the effects of unsteady flow and wing flexion on the relative performance of wings with different planform shapes.

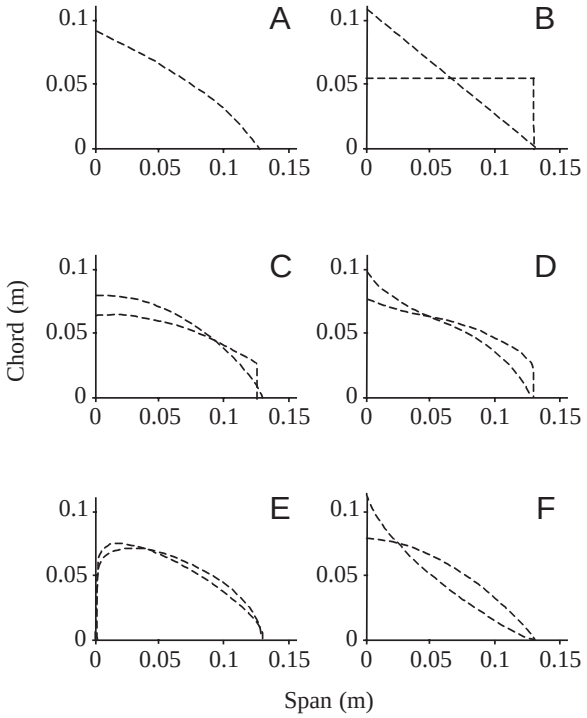

Fig. 2. Chord length distributions of theoretical wings and a ratfish pectoral fin. (A) Chord length distribution of the pectoral fin of the adult ratfish. Total area 0.0069 m^2; aspect ratio 2.2. (B) Sample chord length distributions generated with a first-degree polynomial. (C) Chord length distributions generated with a second-degree polynomial. (D) Chord length distributons generated with a third-degree polynomial. (E) Chord length distributions generated with a beta distribution. (F) Chord length distributions generated with an exponential function. Chord length distributions in B–F represent wings of the same aspect ratio (2.5) and area (0.0069 m^2). See Appendix 2 for the mathematical equations used to generate the theoretical wings.

Results

Ratfish performance and verification of the fluid model

Both ratfish swam at the same forward velocity, and the aspect ratio and wave speed of their pectoral fins are similar (Table 1). The adult ratfish has a larger pectoral fin and flaps with a larger tip amplitude, but the angle subtended by the pectoral fins of the two fish is nearly identical. The juvenile flaps its fins at a higher frequency than the adult, as predicted by mass/frequency scaling relationships noted in aerial animals. The amplitude of the leading edge increases linearly with spanwise position in both the female and the juvenile (r^2>0.98), indicating no significant spanwise bending. The amplitude of the trailing edge of the wing was the same as that of the leading edge at several positions spanwise, so chordwise amplitude change was taken to be zero. Because the movement of the leading edge and chordwise bending of the wing are symmetrical on the up- and downstrokes, the mean angle of attack over the stroke is also zero, so the ratfish do not generate any net vertical force.

The potential flow model indicates that both fish swim with approximately the same locomotor efficiency, but that the adult generates more total thrust (Table 2). This increased thrust may be due to the larger area of the adult's pectoral fins and to the fact that the thrust coefficient for its fins is larger (1.63 in the adult *versus* 1.18 in the juvenile). The thrust calculated using the model is comparable with predicted drag when the measured wave speeds are used, but the thrust calculated for stiff pectoral fins (c=100 m s^{-1}) is considerably higher (Table 2). While the coefficient used to estimate fin drag was measured in steady flow (and thus may not accurately represent the drag on a flapping, bending fin), fin drag accounted for only approximately 10 % of total drag. Thus, even a doubling or tripling of this coefficient will not influence the total drag significantly.

Table 1. *Kinematic and morphological parameters of ratfish*

	Adult	Juvenile
Forward velocity, U ($m\,s^{-1}$)	0.15	0.15
Tip amplitude, H (m)	0.058	0.033
Flapping frequency, f (s^{-1})	1.1	1.6
Wave speed, c ($m\,s^{-1}$)	0.302	0.306
Chordwise amplitude change, ε	0	0
Mean angle of attack, γ (degrees)	0	0
Span, z_0 (m)	0.124	0.068
Angle subtended by fin, Φ (degrees)	27.1	28.1
Fin area, S_p (m^2)	0.0069	0.0022
Aspect ratio, AR (z_0^2/S_p)	2.2	2.1
Body cross-sectional area, S_{cs} (m^2)	0.00551	0.00157

Kinematic variables measured from the lateral view of a swimming ratfish include the forward velocity (U), tip amplitude (H), flapping frequency (f) and wave speed (c) (see Fig. 1).

Chordwise amplitude change (ε) was measured by comparing the amplitudes of the leading and trailing edges at several points spanwise.

The mean angle of attack (γ) was taken to be zero because the kinematics and bending of the fin are symmetrical when averaged over a stroke.

Span (z_0) and the area of one fin (S_p) were measured from the dorsal view of the ratfish and were used to calculate aspect ratio AR.

Span and tip amplitude were used to calculate the angle subtended by the fin (Φ).

The cross section of the body at its widest point was assumed to be an oval, and the cross-sectional area (S_{cs}) was calculated from measurements of maximum body width (from the dorsal view) and depth (from the lateral view).

Table 2. *Model results and calculated drag of ratfish*

	Female	Juvenile
Flexible fin (measured wave speeds)		
Power (W)	0.05	0.01
Efficiency	0.77	0.78
Thrust (N)	0.26	0.06
$Drag_{body+fins}$ (N)*	0.18	0.05
Stiff fin (c=100 $m\,s^{-1}$)		
Power (W)	0.12	0.03
Efficiency	0.58	0.60
Thrust (N)	0.47	0.11
$Drag_{body+fins}$ (N)*	0.18	0.05

The results of the fluid-dynamic model for power output, thrust and efficiency of the female and juvenile ratfish are shown together with the results when a wave speed of 100 $m\,s^{-1}$ is used.

*For comparison, the calculated drag (based on measured coefficients and kinematic variables) for the body plus fins is displayed.

Wing shape parameters

For all wing shapes tested, flapping wings generate more thrust but are less efficient as the proportion of area in the outer part of the wing increases (Fig. 3). This relationship is strongest when performance is plotted against the proportion of area in the outer one-fifth of the wing. The relationship is similar for all four average chord lengths tested, although thrust and efficiency have different asymptotes for each aspect ratio (Fig. 3).

Wings with different shapes but the same amount of area in the outer one-fifth of the wing generate the same amount of thrust and perform with nearly identical efficiency over a range of different average chord lengths (Fig. 4). Thus, aspect ratio and the proportion of area in the outer one-fifth of a wing are sufficient to describe a wing in terms of aerodynamic performance, regardless of the specific details of wing shape.

It should be noted that only wings in which the maximum chord length occurs within the inner one-third of the wing span converge onto the curves in Fig. 3. The performance of wings that continue to increase in chord length past this point diverges from these curves. For the present analyses, we used only wings with the maximum chord located within the inner one-third of the wing.

Relative performance of theoretical wings

High-aspect-ratio wings generate more thrust and are generally more efficient than low-aspect-ratio wings (Fig. 3A,B). Wings with more area distributed to the outer portion of the wing also generate more thrust, but are less efficient than wings with less area in the outer portion (Fig. 3A,B).

As flapping frequency rises, thrust production increases and efficiency generally decreases (Fig. 5), although at higher frequencies and in wings with more area at the tip, efficiency rises and falls with increasing average chord length (Fig. 5D,F). As a result, low-aspect-ratio wings can perform more efficiently than some higher-aspect-ratio wings (in this case, increasing their efficiency by several per cent). In addition, low-aspect-ratio wings flapping at higher frequencies not only can produce more thrust but can also sometimes perform more efficiently than if they were flapping at lower frequencies.

Wings with high wave speeds (e.g. stiffer wings) generate more thrust (Fig. 6A), but are less efficient than those with lower wave speeds (Fig. 6B). In wings with lower wave speeds, efficiency rises and falls by several per cent with increasing average chord length, again showing that low-aspect-ratio wings can be more efficient than high-aspect-ratio wings. The locations of the efficiency peaks (e.g. the locally optimal average chord length) vary with wave speed.

Discussion

Ratfish performance and shape parameters

The potential flow analysis applied to ratfish swimming provides a good estimate of thrust and demonstrates the importance of considering wing and fin flexion in models of animal flight and swimming (because thrust production is overestimated when the fin is assumed to be stiff). Our analyses based on theoretical wing shapes show that aspect ratio and the

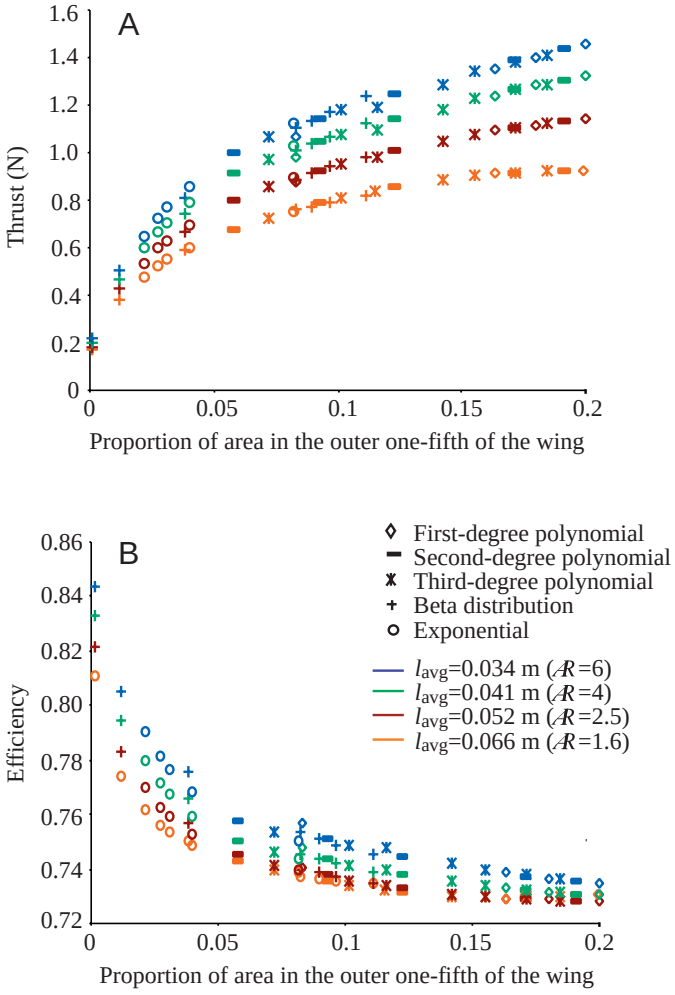

Fig. 3. Performance of theoretical wings generated with the five shape equations *versus* the proportion of area in the outer one-fifth of the wing. Each point represents the performance of one theoretical wing shape. The area of each wing tested is 0.0069 m^2 (multiplied by 2 to give the total performance of an animal). U=0.15 $m\,s^{-1}$, c=0.3 $m\,s^{-1}$, H=0.058 m and f=2.27 s^{-1}. Wing area was fixed, and span was adjusted to create wings with the four specified aspect ratios (AR). (A) Thrust *versus* the proportion of area in the outer one-fifth of the wing. (B) Efficiency *versus* the proportion of area in the outer one-fifth of the wing. U, velocity; c, wave speed; H, fin tip amplitude; f, flapping frequency; l_{avg}, average chord length.

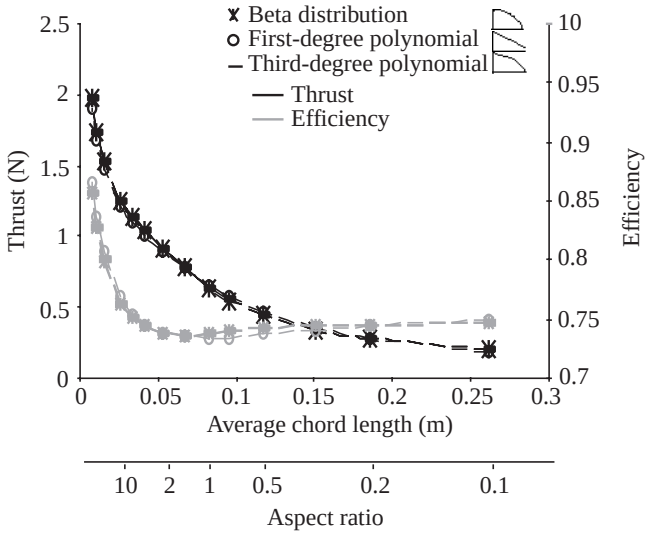

Fig. 4. Thrust and efficiency *versus* average chord length for theoretical wings with different shape, but the same proportion of area in the outer one-fifth of the wing. Wings were generated with three different shape equations: a beta distribution, a first-degree polynomial and a third-degree polynomial. All wings have 9 % of area in the outer one-fifth of the wing. Chord length distributions are also shown. S_p=0.0069 m^2, U=0.15 $m\,s^{-1}$, c=0.3 $m\,s^{-1}$, H=0.058 m and f=2.27 s^{-1}. S_p, total area of one pectoral fin; U, velocity; c, wave speed; H, fin tip amplitude; f, flapping frequency.

proportion of area distributed to the outer one-fifth of the wing are sufficient to characterize wing shape in terms of performance in forward, flapping flight. Thus, aero- and hydrodynamic force generation in forward flight appear to be relatively insensitive to subtle differences in planform wing shape.

While the analyses provide insight into the effects of wing shape on flight performance, the two-dimensional assumption of the fluid-dynamic model places limitations on some of the results. Because the model is essentially a summation of two-dimensional force calculations on strips running from the leading to the trailing edge, spanwise flow is not included. Without this three-dimensional flow, the model cannot predict the effects of tip vortices, which contribute induced drag and influence overall force production. In addition, strong spanwise flow, which may occur at high flapping frequencies, would alter both the overall direction and magnitude of forces and the direction of traveling waves on the wings.

Low-aspect-ratio wings are expected to have larger tip vortices and stronger spanwise flow, so the two-dimensional assumption may become more problematic as average chord length increases (aspect ratio declines). Higher induced drag on these wings will decrease both thrust and efficiency. Including induced drag would affect the values calculated by the model, but will not change the result that multiple peaks in efficiency arise from the interaction between planform shape, unsteady motion and wing or fin flexion.

Interestingly, the impact of induced drag will depend on the reduced frequency parameter. As the reduced frequency parameter increases, bound circulation is expected to decrease because there is not enough time for bound circulation to develop fully before stroke reversal. Thus, induced drag, which is caused by the shedding of bound circulation, will have less of an effect on performance.

Similarly, the predicted values of thrust and efficiency will change when wings are flapped with a non-zero angle of attack (as in aerial flyers that need to support their weight). However, flapping flight with a non-zero mean angle of attack still produces multiple peaks in both efficiency and the thrust coefficient (see Daniel, 1987), although the locations of these peaks may be different from those shown in the figures.

Because the model includes the Kutta condition (in which flow must leave the wing smoothly at the trailing edge), the performance of wings or fins that move with extremely high angles of attack, large amplitudes, high reduced frequency parameters or fast rotations at stroke reversal (motions causing separated flow) cannot be predicted.

Relative performance of wings

We find that thrust and efficiency generally increase in wings with lower average chord lengths (higher aspect ratios), similar to what has been predicted by traditional aerodynamics. However, when flapping frequency is higher and more area is distributed to the outer portion of the wing, efficiency rises and

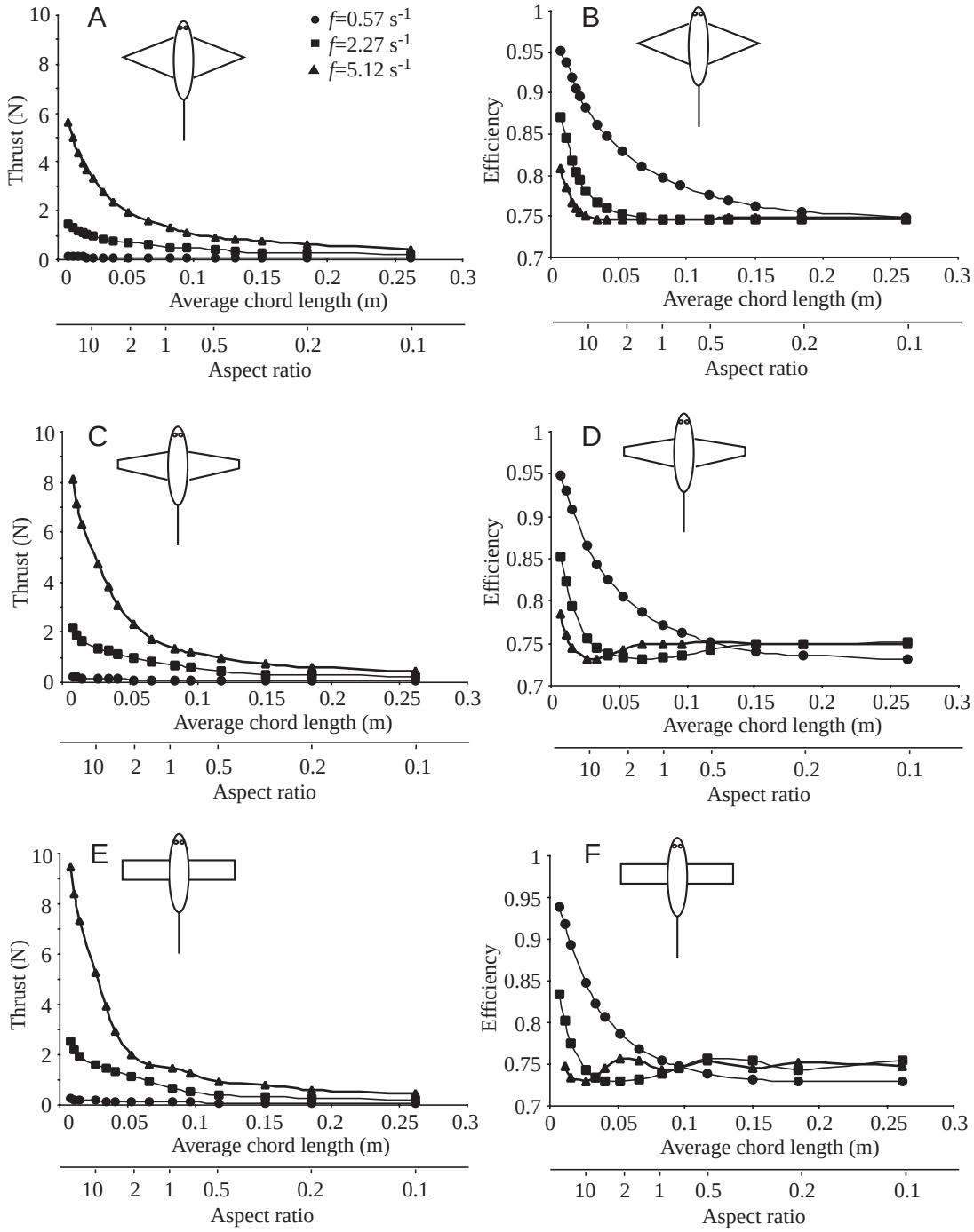

Fig. 5. Performance of theoretical wings at varying flapping frequencies with S_p=0.0069 m^2, U=0.15 m s^{-1}, c=0.3 m s^{-1} and H=0.058 m. All wings were generated with first-degree polynomials. (A,B) Thrust and efficiency *versus* average chord length for triangular wings that have 4% of the wing area in the outer one-fifth of the wing. (C,D) Thrust and efficiency *versus* average chord length for wings that have 12% of the wing area in the outer one-fifth of the wing. (E,F) Thrust and efficiency *versus* average chord length for rectangular wings that have 20% of the wing area in the outer one-fifth of the wing. S_p, total area of one pectoral fin; U, velocity; c, wave speed; H, fin tip amplitude; f, flapping frequency.

falls with increasing average chord length, causing these predictions to break down and suggesting that local performance optima exist.

Both higher flapping frequencies and more area in the outer one-fifth of the wing lead to an increase in the reduced frequency parameter ($\sigma=\omega l/U$) in the outer portion of the wing, a region that contributes strongly to unsteady force production. The effects of this change on thrust production and efficiency can most easily be understood by examining the non-dimensional power and thrust produced by an oscillating strip. As strip length increases (increasing σ), the non-dimensional power and thrust increase initially and then fall into a decaying oscillation (Fig. 7A). Efficiency shows a similar, but complementary, pattern (Fig. 7B), demonstrating a trade-off between thrust and efficiency.

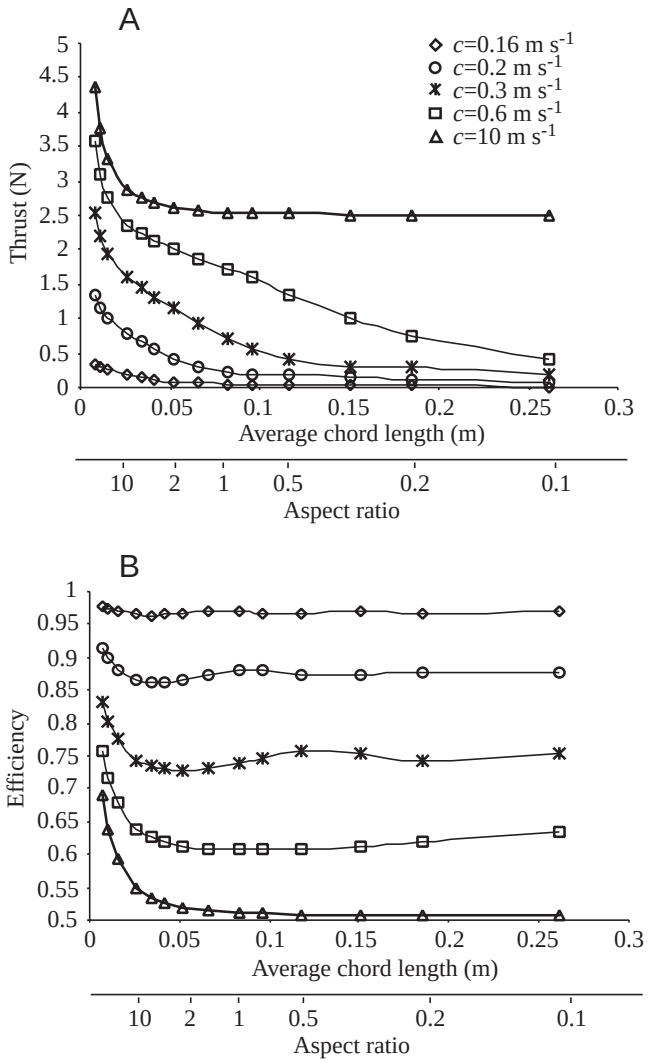

Fig. 6. Performance of theoretical rectangular wings with varying wave speeds. Wings were generated with a first-degree polynomial (20% of the wing area in the outer one-fifth). S_p=0.0069 m^2, U=0.15 m s^{-1}, H=0.058 m and f=2.27 s^{-1}. (A) Thrust *versus* average chord length. (B) Efficiency *versus* average chord length. S_p, total area of one pectoral fin; U, velocity; c, wave speed; H, fin tip amplitude; f, flapping frequency.

These oscillatory behaviors can be explained by the unsteady fluid dynamics inherent in forward, flapping flight. As wing motion becomes more unsteady (for example, as flapping frequency or chord length increases), forces arising from the inertial components of fluid motion increase, causing a rise in inertial thrust production. However, as the reduced frequency parameter increases, the time available for bound circulation to develop decreases, and at some point bound circulation will begin to fall below its full value, causing a decline in total thrust production. As the reduced frequency continues to rise, multiple waves form on the wing and further complicate force production.

While the performance of non-dimensional strips indicates a trade-off between thrust and efficiency, this relationship changes when the strips of a wing are given a finite area and summed. In even the simplest case of rectangular wings (with all strips of equal chord length), the relationship between thrust production and average chord length is not the same as the relationship between non-dimensional thrust production and strip length. While non-dimensional thrust initially rises with increasing chord length and then oscillates as chord length increases further (Fig. 7A), total thrust production by rectangular wings falls continuously as average chord length is increased (Fig. 7C).

This decrease in thrust production can be explained by the fact that, as the average chord length of the wings increases (aspect ratio decreases) with area held constant, more of the wing area is distributed near the base of the wing (because span is decreased). Parts of the wing that are closer to the base undergo smaller accelerations and produce relatively less unsteady, inertial force. Distributing more wing area close to the base (as in low-aspect-ratio wings) therefore results in lower total force production and outweighs the non-dimensional predictions of optimal chord length. In contrast, whole-wing efficiency retains the oscillatory behavior seen in individual strips because efficiency is the ratio of thrust to power; the area terms in the power and thrust equations cancel, and efficiency is determined by the ratio of coefficients, as in the non-dimensional case (Fig. 7D).

The reversal of the relationship between non-dimensional thrust production and strip length when performance is summed over the whole wing changes the non-dimensional prediction of a trade-off between thrust and efficiency into the familiar result that high-aspect-ratio wings generate more thrust and are more efficient than low-aspect-ratio wings. This relationship proves to be more complex, however, in several cases. When the reduced frequency parameter is raised by increasing flapping frequency, oscillations in efficiency become more apparent, and wings with high average chord lengths (low-aspect-ratio wings) can perform more efficiently than those with lower average chord lengths. Distributing more area to the outer portion of the wing (even when average chord length remains the same) produces the same effect. In addition, flapping low-aspect-ratio wings at higher frequencies can

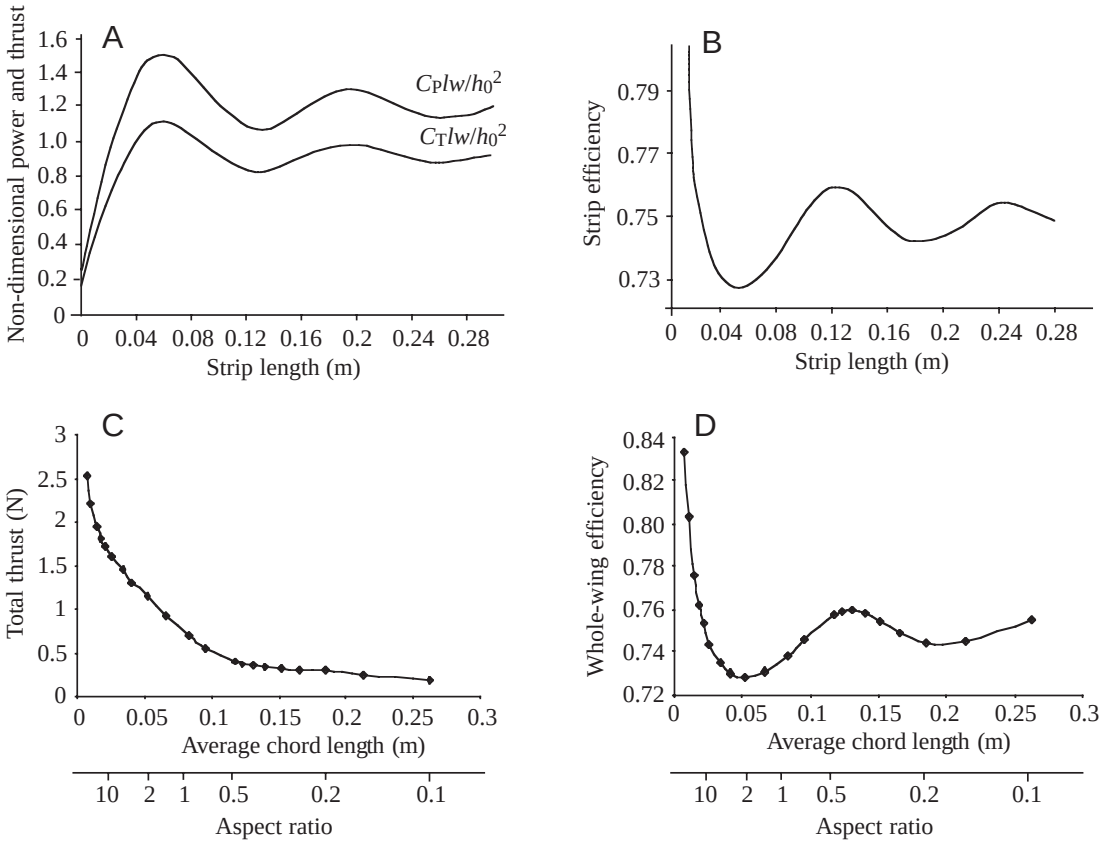

Fig. 7. (A) Non-dimensional power and thrust *versus* strip length. Non-dimensional power and thrust are calculated by multiplying the power or thrust coefficient by strip length and unit width (w=1) and dividing by amplitude squared. (B) Efficiency *versus* strip length. (C) Total thrust produced *versus* average chord length for rectangular wings. (D) Whole-wing efficiency *versus* average chord length for rectangular wings. Each point in parts C and D represents the performance of a single wing with the given average chord length. For all graphs, U=0.15 m s^{-1}, c=0.3 m s^{-1}, H=0.058 m and f=2.27 s^{-1}. U, velocity; c, wave speed; H, fin tip amplitude; f, flapping frequency; C_P, power coefficient; C_T, thrust coefficient; h_0, amplitude; l, strip length.

actually increase both thrust production and efficiency in some cases.

As wave speed decreases, efficiency again rises and falls with increasing average chord length. The overriding effect of decreases in wave speed (e.g. more flexible fins) is to increase efficiency and decrease thrust. But, at lower wave speeds, the local optima in efficiency become more significant, giving some low-aspect-ratio wings a selective advantage over higher-aspect-ratio wings. In addition, the locations of these optima (the average chord lengths that perform best) depend on the wave speed, providing a landscape of evolutionary pressures that could influence various morphological and kinematic features.

Concluding remarks

Our analysis points to several important issues that should be considered in aerodynamic models of flapping flight. First, it reinforces the growing understanding that unsteady effects must be incorporated into models of swimming and flight. Traditional aerodynamic predictions concerning the relative performance of different wing shapes were upheld in this analysis only when the flapping frequency was low or the wing had a relatively tapered tip (a small proportion of area in the outer one-fifth of the wing).

Second, the analysis demonstrates the importance of considering wing flexion in models of flight. While there may be cases where wing flexion is less important (e.g. at lower Reynolds numbers), we find that the thrust generated by a wide range of wings with differing aspect ratios and area distributions will be overestimated and the efficiency underestimated if wings are assumed to be rigid. Furthermore, unsteady effects combined with wing flexion clearly complicate efficiency calculations for flapping wings.

Most importantly, the results point to one possible source of the diversity of wing morphologies and kinematics that exist in nature. The repeated rising and falling of efficiency with increasing chord length suggests that multiple local performance optima exist that may exert subtle selective pressures on the kinematics and morphology of flying and swimming animals. While the predicted changes in efficiency may seem small (Fig. 5D,F, Fig. 6B), an increase in efficiency of a few per cent could, in fact, be critical for animals in many different situations. For example, animals with low energy reserves or those that regularly travel long distances could gain

a large selective advantage if an increase in efficiency allowed them to travel slightly further or decrease their weight by using less fuel than their competitors. In addition, the magnitude of these local optima will vary with different combinations of morphological and kinematic parameters.

The interactions between flight variables (such as wing shape, reduced frequency parameter and wing flexion) show that animals can change many different aspects of kinematics or morphology to reach local peaks in performance. Of course, these selective pressures will interact with many others, such as physical constraints on wing morphology and the interaction between appendage size and maneuverability in complex habitats, to influence the suite of characters that any given animal will display.

The potential importance of wing flexion raises the question of how animals control the bending of their wings and fins during flight. Many vertebrate flyers and swimmers control the bending and flexing of their wings or fins at least partially by muscular activity; the control of these subtle movements on the timescale of a single flap must involve a complex system of feedback and neural control.

Animals with little or no muscular control of wing or fin flexion, such as insects, present an equally interesting challenge. How do these animals control the pattern and timing of the wing deformations that affect flight performance? In animals with little muscular control of wing bending, the evolution of wing shape and the passive flexibility of wings may be linked, and this evolution may be related to the flight style and kinematics of each animal.

Although our analyses focus on planform shape as a determinant of flight performance, the results illustrate that no single feature of flight kinematics or morphology can be studied in isolation. Planform shape, unsteady fluid effects and wing flexion interact in a complex way during flapping flight. In addition, we have not yet explored the effects of unsteady flight mechanisms involving separated flow on the evolution of wing design. However, this study suggests that there are other general patterns in the functional consequences of wing shape that may clarify the relationship between wing morphology, kinematics and flight performance.

Appendix 1 (from Daniel, 1987)

Each segment of the wing is treated as a harmonically oscillating flexible plate centered at the origin. Its motion is prescribed by Equation 1A. The solution of Wu (Wu, 1971) to Euler's equation requires a Fourier representation of the position and velocity of all points on the wing:

$$h(x,t) = \beta_0/2 + \sum_{n=1}^{\infty} \beta_n \cos(n\theta)\,, \tag{A1}$$

where

$$\beta_n = 2/\pi \int_0^{\pi} h(x,t)\cos(n\theta)\mathrm{d}\theta \tag{A2}$$

and

$$V(x,t) = b_0/2 + \sum_{n=1}^{\infty} \beta_n \cos(n\theta)\,, \tag{A3}$$

where

$$b_n = 2/\pi \int_0^{\pi} V(x,t)\cos(n\theta)\mathrm{d}\theta\,. \tag{A4}$$

β represents the Fourier coefficients for wing position, b represents the Fourier coefficients for wing velocity, θ is a variable in the Fourier representation and $V(x,t)$ is the vertical velocity at all points on the surface of the wing, which is given by the material derivative of the instantaneous wing position:

$$V(x,t) = (\partial/\partial t + U\partial/\partial x)h(x,t)\,, \tag{A5}$$

where U is the forward velocity. From these Fourier representations, Wu (Wu, 1971) provides equations for the time-averaged thrust, energy and power coefficients, here defined as:

$$C_P = P_{avg}/(\tfrac{1}{4}\rho\pi U^3 l) = Re(-i\sigma/U)(b_0 + b_1)[(\beta_0^* - \beta_1^*)\Theta(\sigma) + \beta_1^*]\,, \tag{A6}$$

where the asterisk denotes the complex conjugate of the parameter. P_{avg} is the mean power expenditure, $\Theta(\sigma)$ is Theodorsen's function (defined below), *Re* indicates the real part of the enclosed function and ρ is the density of the fluid. C_P is a dimensionless coefficient that represents the total rate at which energy is expended to produce thrust and create vorticity in the wake behind the wing. This latter form of energy dissipation arises from the existence of a jump in the tangential velocity of flow at the trailing edge of the wing. The coefficient for the rate of energy loss by this mechanism is given by:

$$C_E = E_{avg}/(\tfrac{1}{4}\rho\pi U^3 l) = B(\sigma)(b_0 + b_1)(b_0^* + b_1^*)/U^2\,, \tag{A7}$$

where E_{avg} is the mean energy expended in the wake and $B(\sigma)$ is a modified Theodorsen's function. Two functions in Equations A6 and A7 depend on the degree of unsteadiness in the motion. This unsteadiness is given by the parameter σ, called the reduced frequency parameter, which is a measure of the amount of vertical oscillation relative to forward steady motion:

$$\sigma = \omega l/U\,. \tag{A8}$$

The two functions of this parameter, $B(\sigma)$ and $\Theta(\sigma)$, set the time lag in the growth of circulation around the wing. The latter is called Theodorsen's function and is a complex combination of Bessel functions. The former represents portions of Theodorsen's function:

$$\Theta(\sigma) = F + iG = K_1(i\sigma)/[K_0(i\sigma) + K_1(i\sigma)] \tag{A9}$$

and

$$B(\sigma) = F - (F^2 + G^2)\,, \tag{A10}$$

where F is the real part of Theodorsen's function, G is the

imaginary part of Theodorsen's function, i is equal to the square root of −1, and K_0 and K_1 are modified Bessel functions. The function $\Theta(\sigma)$ declines asymptotically from a value of 1 at σ=0 to a value of 0.5 as σ tends to infinity (see Lighthill, 1975). Finally, a coefficient of thrust may be defined by the difference in the coefficients for total power expended and energy lost:

$$C_T = C_P - C_E , \quad \text{(A11)}$$

with an efficiency parameter defined as the rate of useful work done to total power expended:

$$\eta = C_T/C_P . \quad \text{(A12)}$$

Following the appropriate manipulations of the above equations, we arrive at expressions for the coefficients in terms of various Bessel functions. Below are simplified versions of the resultant equations:

$$C_E = 4\beta(\sigma)(\phi_1^2 + \phi_2^2)/U^2 , \quad \text{(A13)}$$

$$C_P = 4\omega(\psi_1\phi_2 + \phi_1\psi_2)/U^2 , \quad \text{(A14)}$$

where

$$\phi_1 = U\varepsilon J_0(\alpha) + (1 - U/c)\omega J_1(\alpha)(h_0 + 2\varepsilon) , \quad \text{(A15)}$$

$$\phi_2 = -U\varepsilon J_1(\alpha) + (1 - U/c)\omega[(h_0 + \varepsilon)J_0(\alpha) + \mu] , \quad \text{(A16)}$$

$$\zeta_1 = (h_0 + \varepsilon)J_0(\alpha) - \mu , \quad \text{(A17)}$$

$$\zeta_2 = -J_1(\alpha)h_0 , \quad \text{(A18)}$$

$$\psi_1 = \zeta_1 F - \zeta_2 G + \mu , \quad \text{(A19)}$$

$$\psi_2 = \zeta_1 G + \zeta_2 F + (h_0 + \varepsilon)J_1(\alpha) , \quad \text{(A20)}$$

$$\mu = \varepsilon[J_0(\alpha) - J_2(\alpha)]/2 , \quad \text{(A21)}$$

$$\alpha = \omega l/c , \quad \text{(A22)}$$

and where J_n is a Bessel function of order n. The central point of these equations is that the performance of this two-dimensional strip, as defined by the coefficients in Equations A11, A13 and A14, depends in a complex manner upon Bessel functions of the parameter α. This parameter is a measure of the number of propulsive waves present on the wing at any instant in time.

Appendix 2

Wings generated with a polynomial distribution were created using equations from Ellington (1984b):

$$\hat{c} = a_0 + a_1\hat{r} + a_2\hat{r}^2 + a_3\hat{r}^3 , \quad \text{(A23)}$$

where $\hat{c}$ is the non-dimensional chord length at any position $\hat{r}$ along the non-dimensional span. The coefficients a_0–a_3 are found by solving the set of simultaneous equations:

$$\hat{r}_k^{\,k} = a_0/(k + 1) + a_1/(k + 2) + a_2/(k + 3) + a_3/(k + 4) , \quad \text{(A24)}$$

with k=0, 1, 2 and 3 and where $\hat{r}_k$ is the radius of the kth moment of area. The first moment of area was taken to be 0.4 (as measured on the ratfish fins) and the second and third moments of area were found from the equations (Ellington, 1984b):

$$\hat{r}_2 = 0.929(\hat{r}_1)^{0.732} , \quad \text{(A25)}$$

$$\hat{r}_3 = 0.900(\hat{r}_1)^{0.581} . \quad \text{(A26)}$$

Wings generated with a beta distribution were also created with equations from Ellington (1984b). The beta distribution is defined for x from 0 to 1 as:

$$f(B) = x^{p-1}(1 - x)^{q-1}/B(p,q) , \quad \text{(A27)}$$

where the beta function $B(p,q)$ is:

$$B(p,q) = \int x^{p-1}(1 - x)^{q-1}dx , \quad \text{(A28)}$$

integrated from 0 to 1. Ellington (1984b) equated f to $\hat{c}$, the non-dimensional chord length, and x to $\hat{r}$, the non-dimensional span. He then defined the parameters p and q as:

$$p = \hat{r}_1\{[\hat{r}_1(1 - \hat{r}_1)/(\hat{r}_2^2 - \hat{r}_1^2)] - 1\} , \quad \text{(A29)}$$

$$q = (1 - \hat{r}_1)\{[\hat{r}_1(1 - \hat{r}_1)/(\hat{r}_2^2 - \hat{r}_1^2)] - 1\} , \quad \text{(A30)}$$

where $\hat{r}_1$ is the radius of the first moment of area and $\hat{r}_2$ is the radius of the second moment of area (found using equation A25, as above).

The last series of wings was created with an exponential equation of the form (Daniel, 1987):

$$l(z) = l_0[1 - (z/z_0)^a] , \quad \text{(A31)}$$

where l_0 is the half chord length at the base, z_0 is the span of the wing and $l(z)$ describes the half chord length at various local positions along the span. The exponent a was varied from 0.01 to 4 to change the shape of the wing.

List of symbols

a	exponent of wing shape in Equation A31
a_0–a_2	polynomial coefficients
AR	aspect ratio
b_0, b_1,...b_n	Fourier coefficients for wing velocity
$B(p,q)$	beta function
$B(\sigma)$	modified Theodorsen's function
c	wave speed
$\hat{c}$	non-dimensional chord length
$C_{D,body}$	coefficient of drag for the body
$C_{D,fin}$	coefficient of drag for one pectoral fin
C_E	coefficient of energy
C_P	coefficient of power
C_T	coefficient of thrust
D_{body}	total drag on the body
D_{fins}	total drag on both pectoral fins
E_{avg}	mean energy expended in the wake
f	flapping frequency
$f(B)$	beta distribution
F	real part of Theodorsen's function
G	imaginary part of Theodorsen's function
h_0	leading edge amplitude
$h(x,z,t)$	local wing position
H	fin tip amplitude

i	$\sqrt{-1}$
J_n	Bessel function of order n
K_0, K_1	modified Bessel functions
l	half chord length
l_{avg}	average chord length
$l_{(z)}$	half chord length at various positions along the span
l_0	half chord length at wing base
n	number of strips
P_{avg}	mean power expenditure
P_{strip}	power expenditure of a chordwise strip of the wing
P_{total}	total power generated by both wings
$\hat{r}$	non-dimensional span
$\hat{r}_k$	radius of kth moment of area
Re	real part of the enclosed function
S_i	surface area of the ith wing strip
S_{cs}	maximal cross-sectional area of the body
S_p	total area of one pectoral fin
t	time
T_{strip}	thrust calculated for a chordwise strip of the wing
T_{total}	total thrust generated by both wings
U	forward velocity
$V(x,t)$	vertical velocity at all points on the wing surface
w	strip width
x	spatial coordinate (spanwise direction)
z	spatial coordinate (chordwise direction)
z_0	span
α	reduced wave frequency parameter
$\beta_0, \beta_1, ...\beta_n$	Fourier coefficients for wing position
ε	chordwise amplitude variation parameter
Φ	flapping angle
γ	mean angle of attack
η	efficiency
η_{strip}	efficiency of a wing strip
η_{total}	efficiency of both wings
θ	variable in the Fourier representation
ρ	fluid density
$\Theta(\sigma)$	Theodorsen's function
σ	reduced frequency parameter
τ	flapping period
ω	circular frequency ($2\pi f$)
ξ	spanwise amplitude variation parameter
*	indicates the complex conjugate of a variable

The authors would like to thank M. Robinson, J. Jensen, B. Miller and K. Liem for their assistance in capturing and filming the ratfish. E. Goldman and M. Tu provided helpful input on drafts of the paper. D. Grunbaum provided invaluable advice on fluid dynamics issues. This work was supported by NSF grant IBN-9511681 to T.L.D., an NSF graduate fellowship to S.A.C., a Friday Harbor Laboratories summer scholarship to S.A.C. and the John D. and Catherine T. MacArthur Foundation.

References

Bestor, C. J. (1993). Pectoral fin locomotion in the spotted ratfish, *Hydrolagus colliei. Friday Harbor Laboratories Fisheries 565 Course Papers*, 1–17.

Blake, R. W. (1983a). *Fish Locomotion*. London: Cambridge University Press.

Blake, R. W. (1983b). Hovering performance of a negatively buoyant fish. *Can. J. Zool.* **61**, 2629–2630.

Blake, R. W. (1983c). Median and paired fin propulsion. In *Fish Biomechanics* (ed. P. W. Webb and D. Weihs), pp. 214–217. New York: Frederick A. Praeger Inc.

Clark, B. D. and Bemis, W. (1979). Kinematics of swimming of penguins at the Detroit Zoo. *J. Zool., Lond.* **188**, 411–428.

Daniel, T. L. (1987). Forward flapping flight from flexible fins. *Can. J. Zool.* **66**, 630–638.

Dickinson, M. H. (1996). Unsteady mechanisms of force generation in aquatic and aerial locomotion. *Am. Zool.* **36**, 537–554.

Dickinson, M. H., Lehmann, F.-O. and Sane, S. P. (1999). Wing rotation and the aerodynamic basis of insect flight. *Science* **184**, 1954–1960.

Ellington, C. P. (1984a). The aerodynamics of hovering insect flight. I. The quasi-steady analysis. *Phil. Trans. R. Soc. Lond. B* **305**, 1–15.

Ellington, C. P. (1984b). The aerodynamics of hovering insect flight. II. Morphological parameters. *Phil. Trans. R. Soc. Lond. B* **305**, 16–40.

Ellington, C. P. (1984c). The aerodynamics of hovering insect flight. V. A vortex theory. *Phil. Trans. R. Soc. Lond. B* **305**, 115–144.

Ellington, C. P. (1995). Unsteady aerodynamics of insect flight. In *Biological Fluid Dynamics* (ed. C. P. Ellington and T. J. Pedley), pp. 109–129. Cambridge, UK: The Company of Biologists Limited.

Ellington, C. P., Van Den Berg, C., Willmott, A. P. and Thomas, A. L. R. (1996). Leading-edge vortices in insect flight. *Nature* **384**, 626–630.

Fung, Y. C. (1990). *Biomechanics: Motion, Flow, Stress and Growth*. New York: Springer-Verlag.

Lighthill, M. J. (1975). *Mathematical Biofluiddynamics*. Philadelphia: Society for Industrial Applied Mathematics.

Liu, H., Ellington, C. P., Kawachi, K., Van Den Berg, C. and Willmott, A. P. (1998). A computational fluid dynamic study of hawkmoth hovering. *J. Exp. Biol.* **201**, 461–477.

Pennycuick, C. J. (1972). *Animal Flight*. London: Edward Arnold (Publishers) Ltd.

Peskin, C. S. (1995). A general method for the computer simulations of biological systems interacting with fluids. In *Biological Fluid Dynamics* (ed. C. P. Ellington and T. J. Pedley), pp. 265–275. Cambridge, UK: The Company of Biologists Limited.

Rayner, J. M. V. (1979). A new approach to animal flight mechanics. *J. Exp. Biol.* **80**, 17–54.

Spedding, G. R. (1992). The aerodynamics of flight. In *Advances in Comparative and Environmental Physiology*, vol. 11 (ed. R. McN. Alexander), pp. 51-111. Berlin: Springer-Verlag.

Sullivan, K. (1979). Mechanical aspects of swimming in the ratfish, *Hydrolagus colliei. Friday Harbor Laboratories Biomechanics (Zool. 533b) Course Papers*, 1–28.

Timoshenko, S., Young, D. H. and Weaver Jr, W. (1974). *Vibration Problems in Engineering*. New York: John Wiley & Sons.

Tong, B.-J., Zhuang, L.-X. and Cheng, J.-Y. (1993). The hydrodynamic analysis of fish propulsion performance and its morphological adaptation. *Sadhana* **18**, 719–728.

Webb, P. W. (1973). Kinematics of pectoral fin propulsion in *Cymatogaster aggregata*. *J. Exp. Biol.* **59**, 697–710.

Weis-Fogh, T. (1975). Flapping flight and power in birds and insects, conventional and novel mechanisms. In *Swimming and Flying in Nature* (ed. T. Y. Wu, C. J. Brokaw and C. J. Brennen), pp. 729–762. New York: Plenum Press.

Wu, T. Y. (1971). Hydromechanics of swimming propulsion. Part 1. Swimming of a two dimensional flexible plate at variable forward speeds in an inviscid fluid. *J. Fluid Mech.* **46**, 337–355.